Investigations of Advanced CO_2 Supersonic Mixing Laser and Propulsion by Laser Absorption

By

Kazuo MAENO*, Hiroshi AOYAMA**,
Akihiro SAKASHITA** and Yutaka HANAOKA*

(September 10, 1988)

Summary: This paper deals with firstly the experimental and analytical approach to advanced scheme of CO_2 supersonic electric discharge laser, and secondly fundamental experiments on propulsion by CO_2 laser absorption. For supersonic CO_2 electric discharge laser, the cluster of supersonic and cylindrical N_2 channels for axial glow discharge are employed, and then conical screen mixing nozzles are used for supersonic mixing of CO_2. Discharge characteristics and supersonic flow properties are measured, along with small signal gain measurement. Vibrationally nonequilibrium analysis of quasi-onedimensional supersonic flow for mixing laser is also conducted, involving N_2 collisional activation by electron impact. Among the results, achievement of steady glow discharge in supersonic N_2 flow is obtained. Measured gain and power dependency on cavity flow distance, on plenum pressures, and on discharge characteristics are discussed in comparison with numerically estimated performances. The duration for maintaining the supersonic flow is about 8 sec that corresponds with our lasing duration. Secondly for the laser propulsion, fundamental experiments with 1 kW-class CW CO_2 laser are conducted. The experimental range is mainly for molecular absorption, and temperature increase is monitored. Among the results obtained, the effect of SF_6 on beam absorption in plenum is remarkable in our experimental conditions.

NOMENCLATURE

A	=	cross sectional area of channel
a	=	sound velocity
C	=	mass fraction
D_f	=	position of lens for laser beam contraction
E	=	electric field
e	=	elementary electric charge
e_i^v	=	vibrational energy of i-th mode
f	=	distribution function of electron energy
G	=	small signal gain coefficient
I	=	laser beam intensity
K_N	=	V-T relaxation rate of N_2
K_{Nv}^e	=	collisional rate for electron-N_2 vibrational activation
k_B	=	boltzmann constant
L_d	=	discharge gap length in N_2 channel
M	=	averaged molecular mass, and also Mach number
m_e	=	mass of electron
N	=	number density
p	=	static pressure in the flow
R_i	=	gas constant of i-th gas
r_{th}	=	nozzle throat radius
T	=	translational temperature

* Department of Industrial Mechanical Engineering, Muroran Institute of Technology
** Graduate Student of Muroran Institute of Technology

T_i = vibrational temperature, and also initial plenum temperature for laser propulsion
T_{ts} = plenum temperature after t sec laser irradiation
u = velocity
v = vibrational level number
V = voltage in electric discharge
W = electric discharge power
X = distance in the mixed cavity
X_i = molar fraction of i-th gas
x = distance in nozzle and cavity
γ = specific heat ratio
ε = electron energy
ε_{Nv} = energy of N_2 vibrational level
ρ = density
θ_N = characteristic vibrational temperature of N_2
σ_j = cross section for j-th inelastic collision
σ_m = cross section for elastic collision
$\sigma_{Nv,v}$ = collisional cross section to v-th vibrational level
η = efficiency

Superscripts
e = electron impact in discharge
n = net quantity
s = stagnation condition
v = vibrational state

Subscripts
C = CO_2
CAV = laser cavity
CF = cathode fall
d = electric discharge
END = plenum conditions after laser irradiation
ex = experimentally measured
H = helium
i = i-th vibrational mode or species, and initial condition for laser propulsion
N = N_2
p = positive column
peak = peak condition with laser irradiation
v = vibrational excitation
1,2,3 = symmetric, bending, and asymmetric mode in CO_2 molecular vibration

1. Introduction

As for the laser technology, many applied researches are flourishing in the fields of space technology, physics, chemistry, medical science, industrial engineering, and so forth. Especially in the space technology, high power lasers are expected as the source of laser energy transmission. Though the wavelength is relatively long, CO_2 laser is one of the most attractive infrared lasers because of its easiness for high power. To obtain the improvement of power and efficiency of CO_2 laser or general high power gas lasers, the large mass flux of population-inverted medium is indispensable. The rise of translational temperature in laser cavity which causes the population increase in lower

laser level should also be restrained. Accordingly, it is favorable to utilize the gas-dynamically supersonic expansion to obtain high power [*1*].

In conventional gasdynamic laser, however, almost all energy is exhausted to produce the high enthalpy supersonic flow even in downstream mixing gasdynamic laser [*2*], [*3*]. If an advanced scheme of CO_2 laser in space is considered, therefore, it is appropriate to employ supersonic expansion from moderate stagnation conditions, which is combined with downstream mixing of independently and electrically excited pumping gas and laser medium. Especially, if longer wavelength for isotope separation or shorter wavelength of CO_2 laser are concerned, low translational temperature in laser cavity should be achieved by supersonic and adiabatic expansion.

This paper deals with an approach to new supersonic CO_2 mixing laser by axial glow discharge in N_2 supersonic channel with the intension of space application [*4*]. Measurement of small signal gain coefficient, along with monitoring electric discharge characteristics, is performed by means of tentative cluster of glass channels for supersonic N_2 discharge and CO_2 conical screen nozzles. A numerical analysis of our supersonic mixing laser by glow discharge based on quasi-onedimensional and vibrationally nonequilibrium flow model is also presented in comparison with experimental results. Furthermore, as the applicational study in space technology, an fundamental experiment for laser propulsion is conducted. Utilizing the conventional 1 kW-class CO_2 CW laser as power source, single conical nozzle is examined for laser absorption phenomena. Temperature and pressure in laser absorbing nozzle plenum are measured. Basic results for test gas mixture of SF_6+N_2 are discussed.

2. CO_2 Supersonic Mixing Laser

2.1 Experimental Setup

Schematic diagram of our experimental setup for supersonic mixing CO_2 electric discharge laser is shown in Fig. 1. The apparatus is designed in consideration that N_2 is vibrationally excited independently in supersonic flow by glow discharge, and afterwards mixed with CO_2 supersonic flow rapidly. The pumping medium N_2 is supplied from tank regulator and solenoid valve into plenum chamber of room temperature, and through 4 conical and supersonic brass nozzles of cathode, the gas exapands into 4 glass tubes (designed Mach number is about 3.4), where axial glow discharge is maintained between these cathode nozzles and anode-block which contains CO_2 screen nozzles. In these tubes N_2 is vibrationally excited by electron impact of supersonic glow discharge, then it is mixed with CO_2 flow which is also expanded from 10 conical supersonic screen nozzles. Laser medium CO_2 is vibrationally excited by molecular collisional activation process (intermolecular V-V transfer) in the mixing region with pumping gas. Cavity size for gain measurement is small with 84x13 mm^2. For DC glow discharge in N_2, 10 kW high voltage power supply is employed.

For the measurement of small signal gain coefficient, CO_2 probe laser (hand-made) and aluminium diffusive reflector are used. Low power beam from reflector is guided

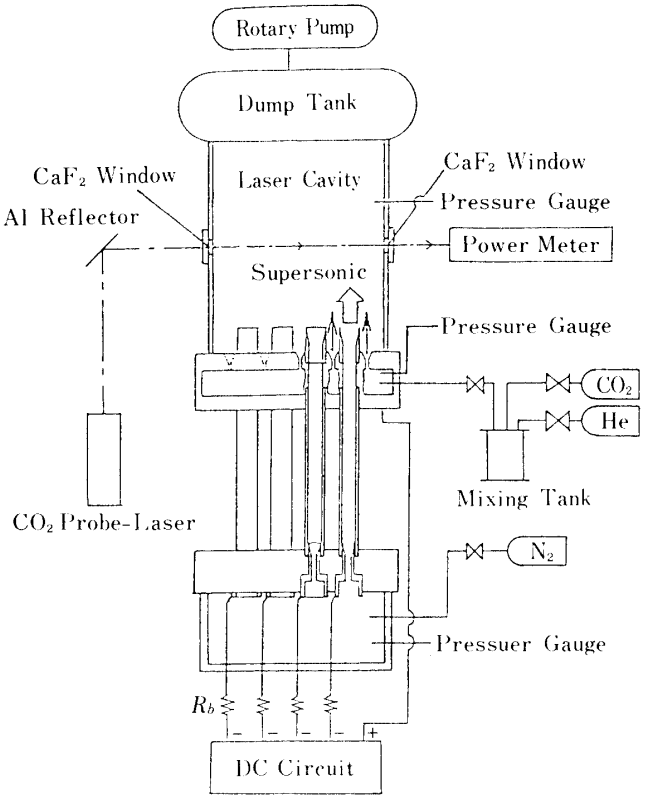

Fig. 1. Experimental apparatus of CO_2 supersonic mixing EDL.

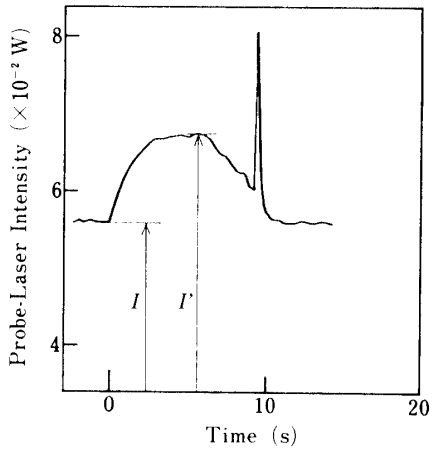

$Q_N = 1.66$g/s
$Q_c = 4.97$
$Q_H = 0.28$
$W_d^n = 288$W
$I = 0.0559$W
$I' = 0.0677$
Gain $= 2.28$m^{-1}

Fig. 2. Typical trace of monitored probe laser power.

through supersonic cavity and detected by thermopile IR power meter. Typical trace monitored by power meter is shown in Fig. 2. It is observed from this figure that the supersonic and population-inverted flow continues about 8 sec, and the augmented beam intensity indicates relatively high gain coefficient. The noise peak from solenoid valve closure is also indicated.

After the population inversion by collisional activation in supersonic mixing, lasing medium CO_2 produces the laser beam from optically stable resonator consisted of total reflecting Si mirror and 90% reflecting Ge partial transmitter at the location of 180 mm (and 200 mm) from CO_2 nozzle exit. The laser beam extracted is monitored by power meter.

The pressures of N_2 and CO_2 reservoirs are monitored by Bourdon's gauges, and the static pressure in supersonic cavity is measured by pirani gauge and pressure transducer. In our experiment Mach number M_{ex} in laser cavity may be calculated by measured static pressure p_{cav} approximately from the following equation:

$$\frac{Q}{A}=\sqrt{\frac{\gamma}{R}}\frac{p_{\mathrm{cav}}}{\sqrt{T^S}}M_{\mathrm{ex}}\left(1+\frac{\gamma-1}{2}M_{\mathrm{ex}}^2\right)^{\frac{1}{2}} \tag{1}$$

where Q is the mass flux by isentropic estimation, R is the gas constant of mixture, and T^S is assumed reservoir temperature of mixed gas.

2.2 Numerical Analysis

To estimate the characteristics of our laser scheme, numerical analysis is performed. The flow shown in Fig. 1 is separated into several sections, which are the separated supersonic expansions of CO_2 and N_2, mixing region from N_2 exit, and mixed cavity flow. According to the assumptions of steady, inviscid, quasi-onedimensional flow, and three-mode relaxation model in molecular system, fluid dynamical equations of mass, momentum, and stagnation enthalpy conservation are formulated, together with the equation of state. Furthermore three vibrational relaxation equations are obtained [5] as;

$$u\frac{de_i^v}{dx}=\Delta E_i \qquad (i=2,\ 3,\ N), \tag{2}$$

These equations are numerically integrated in supersonic expansion sections from throat conditions of vibrational equilibrium. In supersonic N_2 channels of glow discharge, the discharge energy term is added to enthalpy equation, and for N_2 vibrational relaxation equation an additional excitation term is included in the following form;

$$\frac{de_N^v}{dx} = -\frac{K_N}{u}\left\{ e_N^v - \frac{R_N \theta_N}{\exp\left(\frac{\theta_N}{T}\right) - 1} \right\} + \frac{W\eta^e}{\alpha C_N} \quad , \tag{3}$$

$$\eta^e = \eta_P \eta_{Nv}^e \, , \tag{4}$$

$$\eta_P = 1 - \frac{V_{CF}}{V_d} \, , \quad \alpha = \rho u. \tag{5}$$

The discharge efficiency η_p in positive column of glow discharge is estimated by experimental data, and the fractional power transfer efficiency η^e_{Nv} from electron energy to N_2 molecular vibrational energy is given as;

$$\eta_{Nv}^e = \frac{\sum_v^{v_{max}} W_{Nv}}{W} = \frac{\phi_{Nv}\, y}{E v_d} \sum_v^{v_{max}} \varepsilon_{Nv}\, k_{Nv}^e, \tag{6}$$

where y is the mole density and ε_{Nv} is vibrational energy of N_2 level. Discharge current J, discharged power density W, power density W_H for direct Joule heating, power density W_j for j-th inelastic collision, and collisional rate for electron-molecule vibrational activation K^e_{Nv} can be estimated by electron drift velocity and the electron energy distribution function [6], [7], [8].

As the dependence of collisional rates for molecular vibration on vibrational levels is weak, and cross section is dominated by electron energy loss, the molar fraction related to j-th inelastic collisional process can be given by N_2 molar fraction X_N, and cross sections are calculated by the activational data from the ground level. The maximum vibrational activation level v_{max} is assumed to be eight [9].

The electron energy distribution function is calculated by numerical integration of the simplified, isotropic, and steady-state Boltzmann equation for electron energy [10] in N_2(+He);

$$\begin{aligned} &\frac{1}{3}\left(\frac{E}{y}\right)^2 \frac{d}{d\varepsilon}\left(\frac{\varepsilon}{\sigma_{m1}}\frac{df}{d\varepsilon}\right) + \frac{2m_e}{M}\frac{d}{d\varepsilon}\left(\varepsilon^2 \sigma_{m2} f\right) + \frac{2m_e k_B T}{Me}\frac{d}{d\varepsilon}\left(\varepsilon^2 \sigma_{m2}\frac{df}{d\varepsilon}\right) \\ &+ \sum_j (\varepsilon + \varepsilon_j) f(\varepsilon + \varepsilon_j) \phi_j \sigma_j (\varepsilon + \varepsilon_j) - \varepsilon f(\varepsilon) \sum_j \phi_j \sigma_j(\varepsilon) \\ &+ \sum_j (\varepsilon - \varepsilon_j) f(\varepsilon - \varepsilon_j) \phi_{-j} \sigma_{-j} (\varepsilon - \varepsilon_j) - \varepsilon f(\varepsilon) \sum_j \phi_{-j} \sigma_{-j}(\varepsilon) = 0 \, , \end{aligned} \tag{7}$$

$$\int_0^\infty \varepsilon^{(1/2)} f(\varepsilon)\, d\varepsilon = 1 \, , \quad \bar{\varepsilon} = \int_0^\infty \varepsilon^{(3/2)} f(\varepsilon)\, d\varepsilon \, , \quad \bar{\varepsilon}_r = \frac{2}{3}\bar{\varepsilon} \tag{8}$$

After integration of these vibrational nonequilibrium system with glow discharge to the discharge exit, finite length mixing model is adapted to supersonic mixing of N_2 and CO_2 flows. The flow from N_2 exit is partitioned into N_2 side, CO_2 side, and mixed stream side. Algebraic and differential equations describing the three regions are solved to give the flow parameters. Starting from these obtained parameters, non-equilibrium mixed flow in laser cavity is further solved numerically.

2.3 Results and Discussion for CO_2 Laser

A) Discharge Characteristics

The typical discharge characteristics obtained in our experiment are shown in Fig. 3. Steady DC glow discharge in supersonic N_2 flow is attained from almost constant discharge voltage and linearly increasing discharge power. Measured discharge voltage dependence on nitrogen reservoir pressure is indicated in Fig. 4. Since the pressure in discharge region is related directly to N_2 reservoir pressure for fixed nozzle shape, chathode fall can be obtained from the proportional relation between the pressure of discharge channel and net discharge voltage, which enables us to estimate the net power that is actually consumed in electrical impact excitation of N_2.

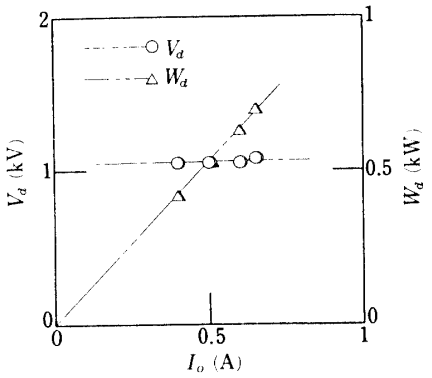

L_g=100mm
L_p= 50
L_d= 50
p_C^s=101.3kPa
p_N^s=34.7
P.M.: Bs (+Al wire)

Fig. 3. Discharge characteristics.

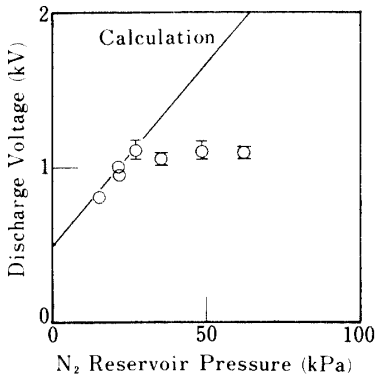

L_d=50.0mm
P.M.: Bs (+Al Wire)
p_C^s=61.3kPa

Fig. 4. Discharge voltage dependence on N_2 reservoir pressure.

B) Numerical Results

As the first result of our numerical estimation, Fig. 5 indicates the temperature distributions in conical CO_2 nozzles. From the moderate plenum conditions, vibrational temperatures $T_{1,2}$ and T_3 are almost frozen of small difference from throat temperature. The translational temperature T, however, decayes rapidly from throat. In this analysis no condensation effect is assumed as vibrational temperatures are frozen to be high values. The supersonic N_2 flow is also frozen tightly to the throat conditions.

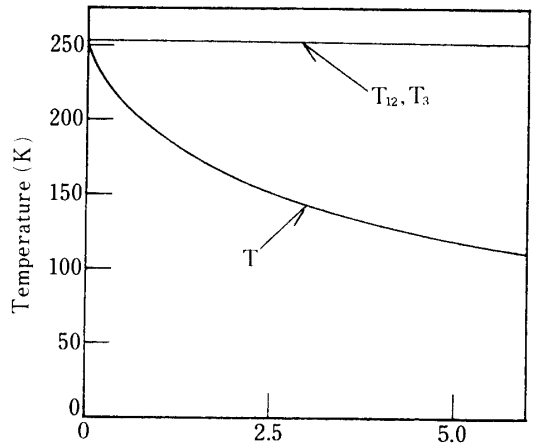

$p_C^s = 39.5$ (kPa), $T_C^s = 293$ (K)
$r_C^* = 1.0$ (mm), $r_C = 2.5$ (mm)
$A_C / A_C^* = 6.25$

Fig. 5. Translational and vibrational temperature distributions in CO_2 nozzle.

In DC glow discharge analysis, Fig. 6 presents the calculated electron energy distribution functions for N_2(+He) under typical E/N of 3×10^{-20} Vm^2. It is remarked that the distribution function is composed into the equilibrium one as molar fraction of helium is increased. Under the experimental conditions, E/N ranges from 3 to 4 ($\times 10^{-20}$ Vm^2), where vibrational excitation is effectively obtained by electron impact. The distributions of translational and vibrational temperatures in N_2 supersonic glow discharge section are indicated typically in Fig. 7. As expected, low translational temperature in supersonic and adiabatic expansion channel and rapid increase of vibrational temperature by N_2 glow discharge are realized. Typical distributions of other flow parameters in this discharge channel are indicated in Fig. 8. The ascent of the pressure and the gradual descent of Mach number are originated from Joule heating of nitrogen gas, that is going to choke the supersonic flow with increasing the input power excessively.

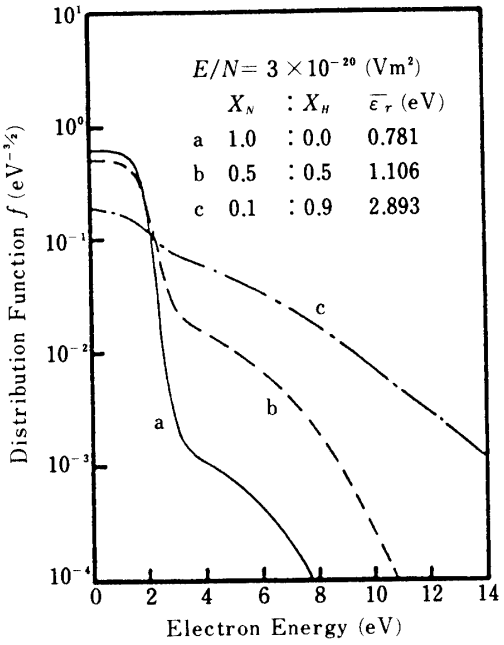

Fig. 6. Electron energy distribution function in N_2 and He mixture.

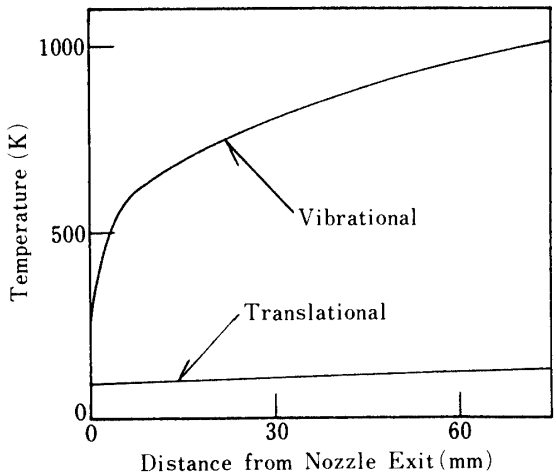

$p_N^s = 33.3$ (kPa)
$L_d = 75.0$ (mm)
$W_d = 150$ (W)
$E/N = 0.39 \times 10^{-19}$ (Vm²)
$\eta_{Nv}^e = 0.94$

Fig. 7. Translational and vibrational temperature distributions in N_2 discharge section.

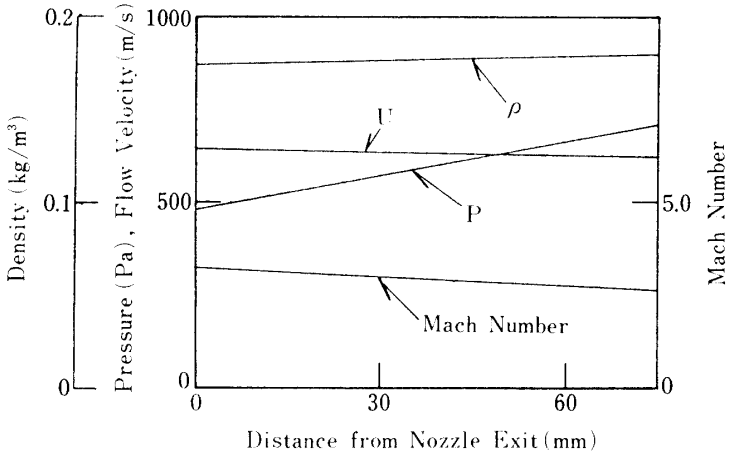

$p_N^s = 33.3$ (kPa), $L_d = 75.0$ (mm), $W_d = 150$ (W)
$E/N = 0.39 \times 10^{-19}$ (Vm^2), $\eta_{Vr}^c = 0.94$

Fig. 8. Flow parameters in N_2 discharge section.

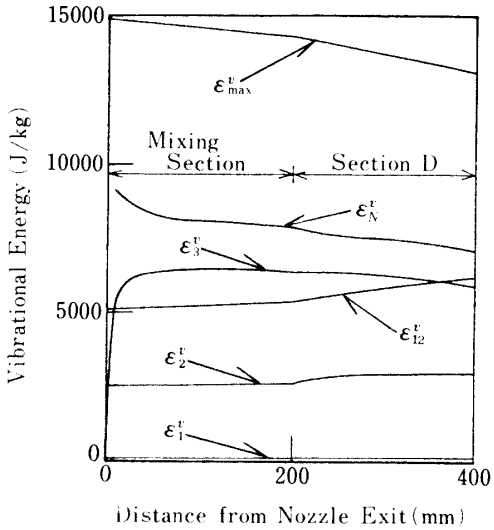

$p_C^s = 39.5$ (kPa), $p_N^s = 33.3$ (kPa)
$V_d = 1800$ (V), $L_d = 75.0$ (mm)
$W_d = 150$ (W)
$E/N = 0.39 \times 10^{-19}$ (Vm^2)
$\eta_{Vr}^c = 0.94$

Fig. 9. Distribution of vibrational energy in cavity along flow direction.

As for the mixed cavity flow region, distributions of vibrational energy along the flow direction are indicated in Fig. 9, where ε^{v}_{max} is the total of energies of CO_2 upper laser level and N_2. From this figure it is remarked that effective energy transfer from electrically excited N_2 molecule to $CO_2(\nu_3)$ is accomplished in the mixing section. In our estimation the distance of mixing section was decided from experimental flow visualization, where the luminescence of glow-discharge-activated nitrogen flow made us possible to visualize the mixing supersonic flows.

C) Experimental Results and Comparison with Numerical Estimation

In regard to the experimental results for flow parameters, Fig. 10 represents the dependence of Mach number on N_2 reservoir pressure, where M_{is} is calculated by isentropic relation for premixed gas from cross-sectional area ratio, and M_{im} is estimated by instantaneous mixing assumption of isentropically calculated flows which indicate not so great difference from vibrationally nonequilibrium estimation. In the figure they present a large discrepancy from M_{ex} that calculated from measured pressure by the previous equation. The main considerable reasons are the mixing loss of N_2 and CO_2 supersonic flows which is caused mainly by pressure waves and vortices, and decreasing cavity supersonic flow due to the development of boundary layer on rectangular cavity walls. The isentropic assumptions, of course, are not sure for electrically discharging nonequilibrium flow.

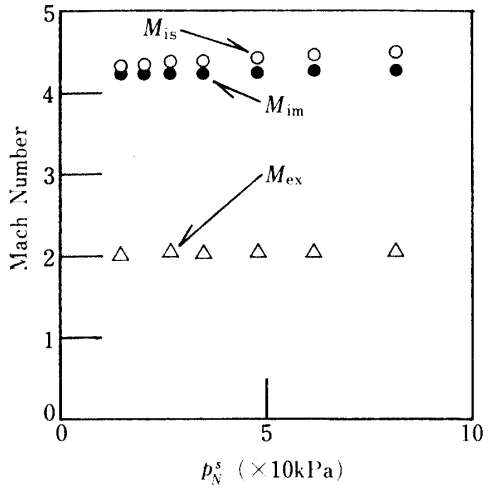

Fig. 10. Dependence of Mach number in cavity on N_2 reservoir pressure.

Measured cavity pressure and laser power typically extracted are presented in Fig. 11. Immediately after the opening of solenoid valves, N_2 and CO_2 are introduced into the laser cavity, and the static pressure p_{cav} maintains constant value about eight seconds before a steep increase, which shows the achievement of supersonic flow. This pressure variation is in accordance with the laser beam extraction as shown in the same figure.

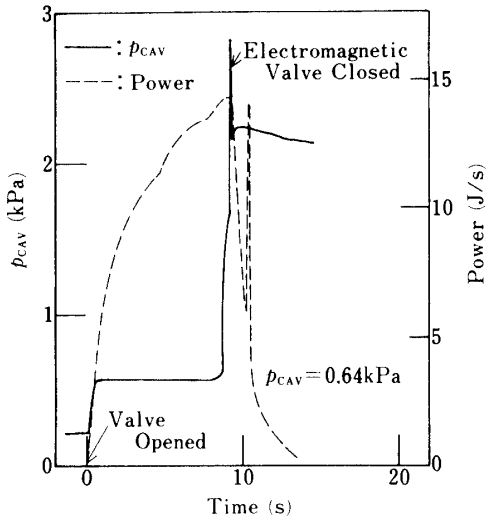

X =205mm
p_C^s=81.3kPa
p_N^s=34.7

Fig. 11. Time variations of cavity pressure and extracted laser power.

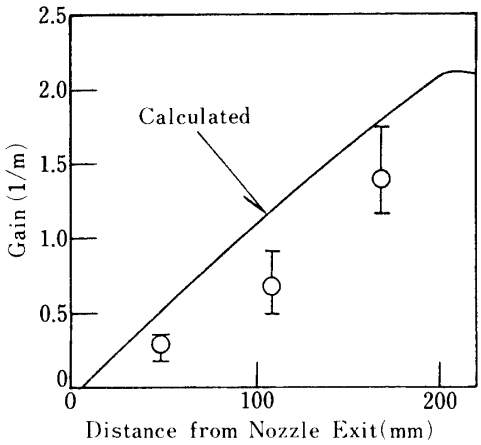

p_C^s=39.9(kPa), p_N^s=13.3(kPa)
T_C^s=T_N^s=293(K)
L_d=75.0(mm)
W_d=150(W)

Fig. 12. Typical gain distribution along flow direction.

On the small signal gain distribution along the flow direction, Fig. 12 indicates the augmenting tendency of measured and estimated gains in accordance with linear increase of mixed flow region, which may correspond to turbulent mixing of supersonic flows. In our' experiment high positive gain distribution is obtained without any deactivation catalyst (He nor H_2O) as shown in the figure. This gain without catalyst originates from low distributions of translational temperature and vibrational temperature of

lower laser levels from moderate plenum conditions.

Figure 13 shows the gain dependency on N_2 plenum pressure with fixed CO_2 reservoir at fixed position in laser cavity. The agreement of measured and estimated results is satisfactory in this discharge conditions. In Fig. 14 the gain characteristics on N_2 reservoir pressure ratio p^S_C/p^S_N is also indicated. It is remarked from this figure that high pressure ratio of CO_2 is distinctive as compared to the low CO_2 fraction of conventional CO_2 gasdynamic laser (GDL) or electric discharge laser (EDL). The appropriate plenum pressure ratio is from 2 to 4 in our laser scheme without helium.

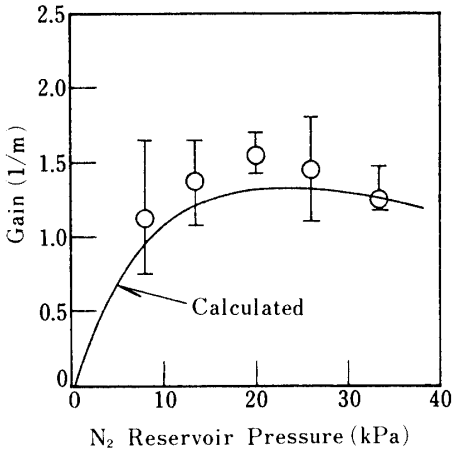

$p_C^s = 53.3$ (kPa)
$L_d = 50.0$ (mm)
$X = 170$ (mm)
$W_d = 150$ (W)

Fig. 13. Gain chararcteristics on N_2 reservoir pressure at fixed position in cavity.

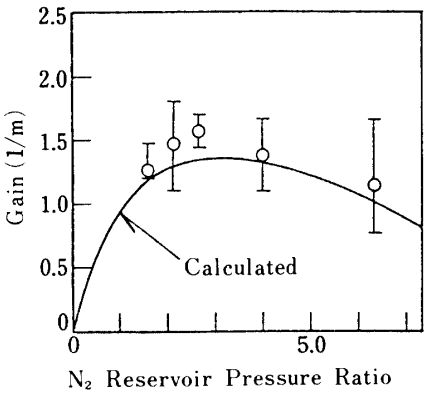

$p_C^s = 53.3$ (kPa)
$L_d = 50.0$ (mm)
$X = 170$ (mm)
$W_d = 150$ (W)
$V_{CF} = 700$ (V)

Fig. 14. Gain characteristics on CO_2 reservoir pressure ratio at fixed position.

D) Application of Advanced CO_2 Laser to Laser Propulsion

Employing the advanced scheme of above-mentioned CO_2 laser, applications to space energy transmission can be considered, although the wavelength of CO_2 laser is relatively long and the distance of energy transmission is not so long up to 1000 km. As for the laser propulsion concept by CO_2 laser [*11*], [*12*], the favorable specific impulse range of 500–2000 sec for orbital transfer of subsatellite can be attained. Figure 15 represents the block diagram of our closed cycle CO_2 mixing EDL for the early stage experiments of laser propulsion in space. For our scheme of supersonic mixing EDL, of course, the much greater power level of few megawatts is suitable, whose range cannot be achieved by conventional CO_2 EDL. From the figure, if the CO_2 laser power required for the experiment is considered to the 3 kW, the total mass flux pumped by the turbocompressor may be 150 g/s, the discharged power density in N_2 flow should be about 200 J/g, and total power supplied by solar cells array is above 30 kW. In typical specs of this laser propulsion experiment, the distance of the subsatellite from the station in space is ranged within 100 km, and the tracking resolution can be assumed to be 0.01 mrad, so the diameters of Cassegrain transmitter on the station and receiver satellite become 2–3 meters.

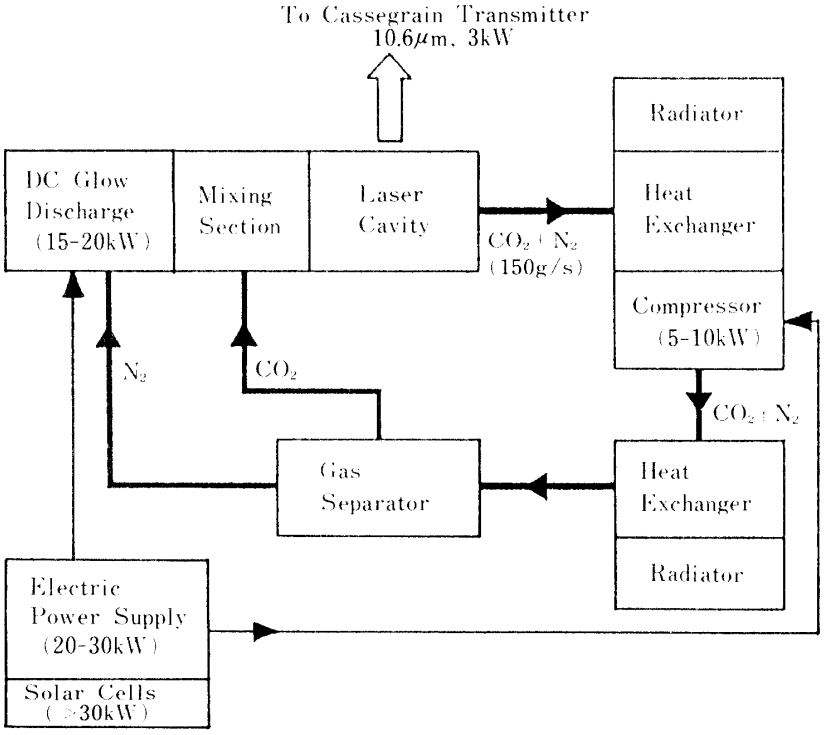

Fig. 15. Schematic diagram of closed cycle CO_2 mixing EDL in space application

3. Laser Propulsion Experiment by CW CO_2 Laser

3.1 Experimental Apparatus

In connection with the laser propulsion, fundamental experiments are conducted. Figure 16 shows the schematic diagram of our experimental setup. The CW CO_2 laser (Shimada Rika Co. Ltd., A-10) of IRI (Industrial Research Institute). The experimental setup consists of nozzle section, IR optical instruments, gas supplying ports, and evacuation and cooling system. As for the nozzle section, upstream subsonic section is glass tube of 11.2 mm inner diameter and 80 mm length for flow visualization. In this glass pipe section, laser beam is concentrated to produce high enthalpy conditions. Through the glass tube the test gas is heated up and then expands by convergent-divergent nozzle into evacuation chamber. The brass convergent-divergent nozzle block is removable and the several substitutable nozzles (of 0.4 – 1.5 mm throat diameter) are employed. Figure 17 presents the dimensions of nozzle section.

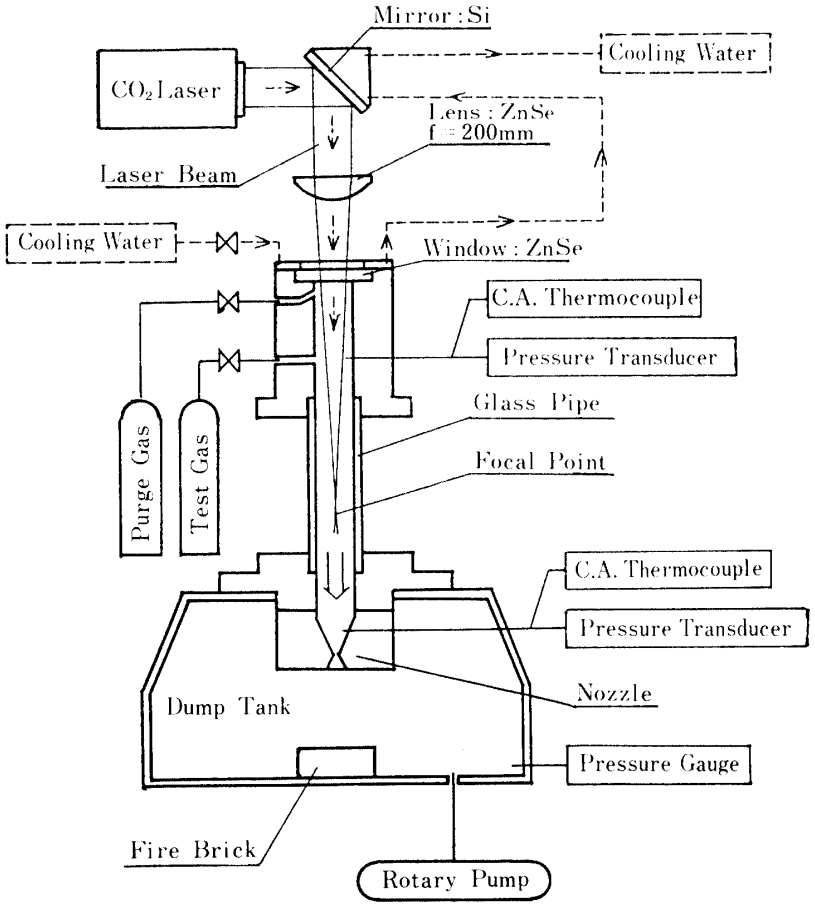

Fig. 16. Schematic diagram of experimental appratus for laser propulsion.

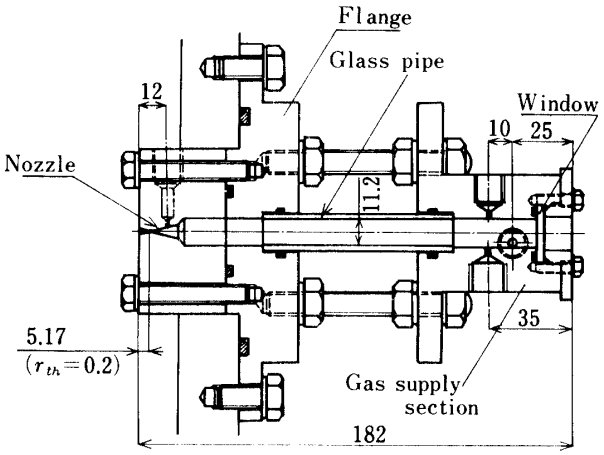

Fig. 17. Diagram of nozzle-plenum assembly for laser propulsion.

The upstream section of the glass tube is Bs gas supplying portion of 12 mm inner diameter and 65 mm length. The upper end is ZnSe window for IR light induction. Purge gas is supplied from control valve through two pipes of 4 mm inner diameter that are directed to the inner surface of ZnSe window at 10 mm downstream from the window. Through the pipe of 2 mm inner diameter at 20 mm downstream from the window the test gas is supplied into subsonic plenum chamber. The port for pressure or temperature measurement is also located at same position, and another measuring port is located at about 7 mm upstream from the nozzle throat.

For introduction of IR laser beam from CW laser source into the glass plenum, Si total mirror of 1 inch diameter for beam reflection, ZnSe lens of 1 inch diameter and 200 mm focal length, and ZnSe window of 1 inch diameter are set on the upstream portion of the glass tube. With adjusting the distance of the ZnSe lens from our nozzle apparatus, the focal point in glass tube can be controlled. The whole view of laser propulsion experimental setup is presented in Fig. 18.

The evacuation chamber has about 34 litres volume and evacuated by rotary pump (ULVAC D-650). In the chamber a fire brick of laser beam damping is settled. The Si total reflector and ZnSe window of nozzle upper portion are cooled by water pipe made of copper. The leakage test ensured us the leak ratio of 1.3 Torr during 30 minutes.

Flow parameters in laser heated plenum are measured by CA sheath thermocouple and pen-recorder (Rika-denshi Co., Ltd., SP-H5P) for temperature, and by pressure transducer (Kyowa, PH-10KA) and oscilloscope (Hitachi-Electr., VC-6041) for pressure variations. The pressure in evacuation tank is monitored by 1.5-class Bourdon's gauge.

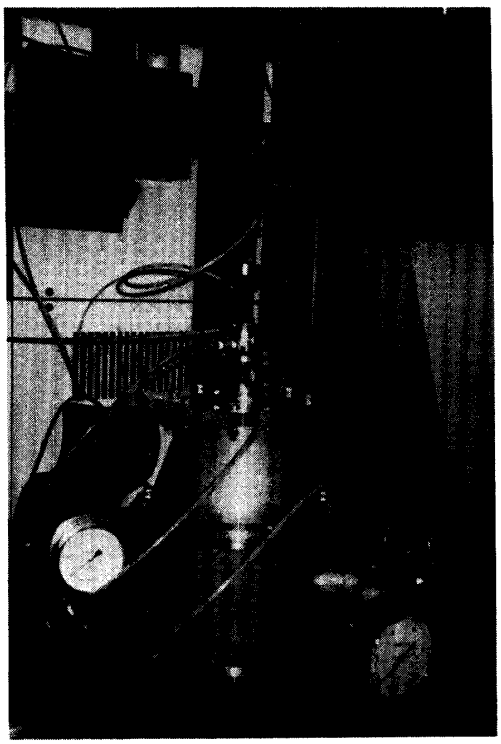

Fig. 18. Whole view of experimental setup for laser propulsion.

3.2 Results and Discussion

A) Luminescence of Test Gas by Laser Beam Absorption

In our experiments by the test gases of SF_6 or R-12, the luminescence of the gas is observed by irradiation of laser beam. Figure 19 shows the photograph of such luminescence by IR beam absorption. The experimental conditions in the figure were:

Test gas; $SF_6 + N_2$,	Molar fraction of SF_6; 50%,
Mass flow rate; 13.1 g/s,	Throat radius; 0.2 mm,
Laser beam power; 500 W,	Beam duration; 11 sec.

As shown in Fig. 19, the luminescence color is white-blue, and the luminous area is almost whole region that is irradiated by beam concentration. This experimental result, therefore, indicates the molecular resonance absorbtion of CO_2 laser beam by SF_6, as compared with the another experimental results of strong light emission from laser absorbed plasma. In this experiment, however, temperature increase of about 130 K in plenum chamber was observed, which is comparable to the preliminary results of laser plasma experiments.

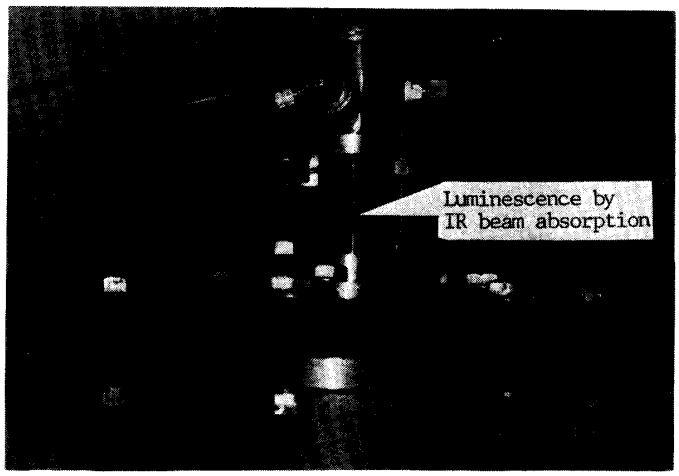

Fig. 19. **Light emission from IR laser-absorbed SF_6 in laser propulsion instrument.**

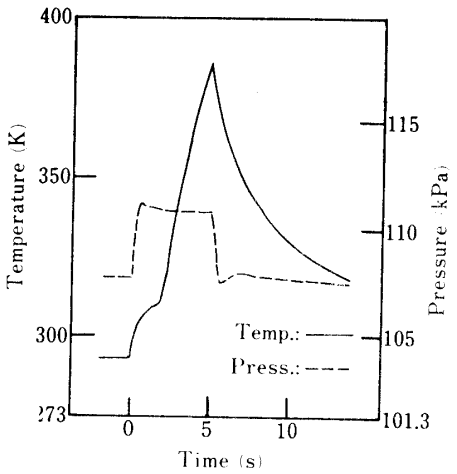

Power = 500W
Mass flux = 13.7g/s
Gas: $SF_6 + N_2$
$X_{SF_6} = 0.51$
D_t 151mm
$r_{th} = 0.2$mm

Fig. 20. Time variation of temperature and pressure of SF_6+N_2 mixture in plenum chamber.

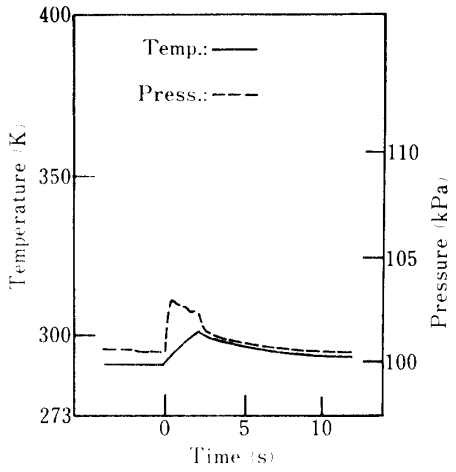

Power 700W
Mass flux = 7.3g/s
Gas: N_2
D_t = 151mm
r_{th} 0.2mm

Fig. 21. Time variation of temperature and pressure of pure N_2 test gas.

B) Time Variation of Flow Parameters

Typical time variations of temperature and pressure in plenum chamber are shown in Fig. 20. The temperature is monitored at 20 mm downstream from the ZnSe window (on the opposite side of gas supplying port), and pressure is measured at the port about 7 mm upstream of nozzle throat. In the figure the temperature begins to increase immediately after the irradiation of laser beam, and continues to increase during the beam irradiation. The pressure, on the other hand, augments quickly after the beam introduction, and keeps the constant value during the beam irradiation. In case

of pure N_2 test gas, the increase of plenum temperature and pressure are small as indicated in Fig. 21. Clearly these results correspond to molecular resonance absorption of laser beam by the test gas including SF_6.

C) Effect of Inclusion of SF_6

The temperature increase in plenum chamber at 1.0 sec after initiation of laser irradiation is shown in Fig. 22 with respect to SF_6 molar fraction. In Fig. 23 the temperature increase at 2.0 sec is indicated. From these figures it is remarked that the temperature rise from initial state is augmented with increasing the molar fraction SF_6 and with increasing the input beam energy. This is mainly due to the molecular absorption of laser energy by SF_6 whose absorption lines involve the wavelength of CO_2 laser. As for the pressure in plenum, Fig. 24 presents the difference of peak value of pressure with laser introduction from initial conditions with respect to SF_6 molar fraction. The same trend as shown in Figs. 22 and 23 can be observed.

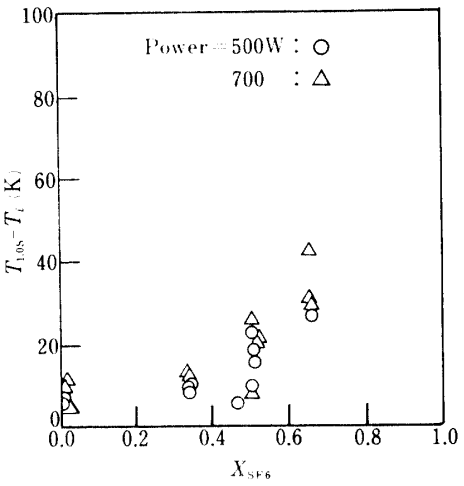

Fig. 22. Temperature increase in plenum at 1.0 sec after laser irradiation with respect to molar fraction of SF_6.

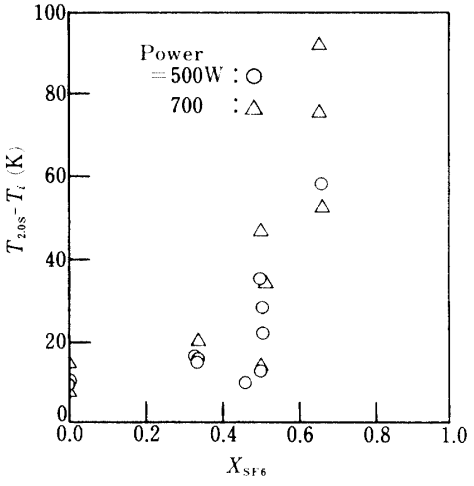

Fig. 23. Temperature increase in plenum at 2.0 sec after laser irradiation with respect to SF_6 molar fraction.

With regard to the flow parameters on absorbed laser energy, Fig. 25 indicates the temperature rise from initial conditions with respect to total energy input for SF_6 molar fraction of 0.5. Initial plenum pressure is the parameter in the figure. The almost linearly increasing tendency with input energy can be seen, which becomes more clear as the initial plenum pressure is augmented. In our experiment the appropriate initial pressure range in plenum chamber is 150 kPa from the figure. The results for pressure of 200 kPa is somewhat different with low distribution, which should be checked in more detail. If the test gas does not involve SF_6 in our arrangement, the

increase in plenum temperature is seemed to be small without the molecular vibrational absorption effect. Figure 26 shows the results for pure N_2 test gas. As expected, the temperature augmentations are quite small in comparison with the results in the previous figure.

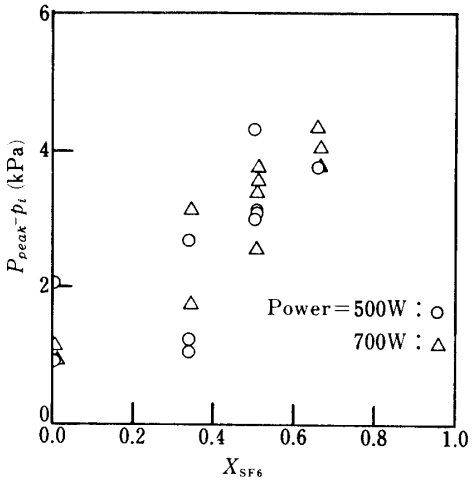

Mass flux=5-20g/s
Gas: SF_6+N_2
$D_f=151$mm
$r_{th}=0.2$mm
$T_i=291.2-302.3$K

Fig. 24. Dependence of pressure peak increase in plenum on SF_6 molar fraction.

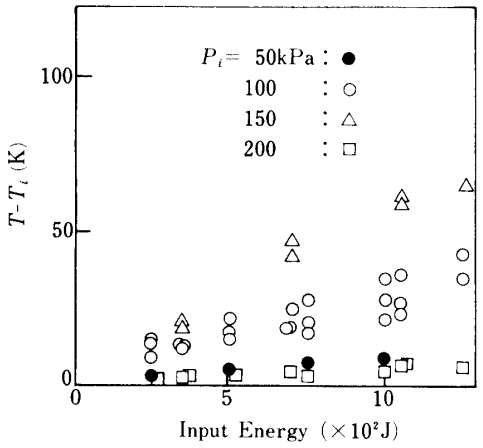

$X_{SF6}=0.5$
Mass flux=5-20g/s
Gas: SF_6+N_2
$D_f=151$mm
$r_{th}=0.2$mm
$T_i=291.2-302.3$K

Fig. 25. Dependency of temperature increase on total input energy for SF_6+N_2 mixture.

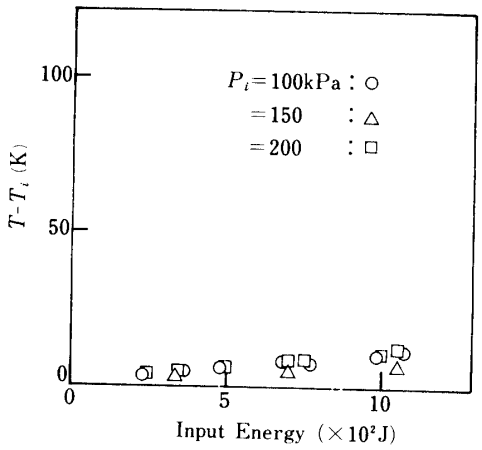

$X_{SF6}=0$
Mass flux=5-10g/s
Gas: N_2
$D_f=151$mm
$r_{th}=0.2$mm
$T_i=297.6-298.2$K

Fig. 26. Dependency of temperature increase on total input energy for pure N_2 test gas.

4. Concluding Remarks

With considering the space application, experimental and analytical investigation on supersonic CO_2 mixing laser by axial glow discharge in supersonic N_2 channel is conducted. Measurement of small signal gain coefficient is performed, together with monitoring the discharge characteristics, from which the steady glow discharge in supersonic nitrogen flow is confirmed. Numerical estimation for vibrationally nonequilibrium flow with electric excitation effect is also presented, which indicates the high gain distributions under the experimental conditions. The optimum operating conditions at higher CO_2 molar fraction than conventional gasdynamic CO_2 GDL can be obtained. Deactivation catalyst helium does not bring forth the positive effect in our scheme. Gasdynamic parameters in supersonic mixing CO_2 EDL are numerically studied in detail.

With regard to the advanced propulsion by laser beam absorption, basic experiments with 1 kW-class CW CO_2 laser are conducted. The obtained results in our experimental range are not for the laser heated plasma but are mainly for the molecular vibrational absorption by SF_6 involved in test gas. The effect of SF_6 on laser beam absorption in plenum chamber is studied in our experimental conditions.

5. Acknowledgement

The authors are grateful to express their sincere thanks to Mr. M. Hirose of Fuji Heavy Industries for his assistance in our experiments and numerical analysis for CO_2 mixing EDL, and also to Mr. K. Shimizu and his colleagues of IRI Laser Laboratory of Industrial Research Institute for his support in numerical calculation for CO_2 mixing EDL and their discussion and experimental support in CW laser source. Also the authors wish to express many thanks to Prof. K. Kuriki and Emeritus Prof. H. Oguchi ISAS for their discussions and experimental support in CO_2 mixing EDL and in ı ɔr propulsion.

References

[' J. D. Anderson, Jr., "Gasdynamic Lasers: An Introduction," *Academic Press,* NY (1976).

[. P. E. Cassady, A. L. Pindroh, and J. F. Newton, "Performance Potential of Advanced GDL Concepts," *AIAA Journal,* Vol. 17, No. 8 (1979), pp. 845–853.

[3 K. Maeno, K. Funabiki, and H. Oguchi, "Experimental and Analytical Study of CO_2/N_2 Mixing Gasdynamic Laser," *ISAS Report* (No. 593), Vol. **46**, No. 5 (1981), pp. 175–197.

[K. Maeno, "CO_2 Gasdynamic Laser and Its Improvement in Space Technology," *Proceedings of the 2nd ISAS Space Energy Symposium,* ISAS (1982), pp. 218–224.

ı K. Maeno and N. Yamaguchi, "An Investigation of Supersonic Mixing CO_2 Electric Discharge Laser," *Proceedings of the 5th International Symposium on Gas Flow and Chemical Lasers, Institute of Physics,* Conference Series No. 72, Adam Hilger Ltd., Bristol and Boston (1985), pp. 419–424.

[6 T. H. Johnson, L. J. Palumbo, and A. M. Hunter, "Kinetics Simulation of High-Power Gas Lasers," *IEEE Journal of Quantum Electronics,* Vol. **QE-15**, No. 5 (1979), pp. 289–301.

[7] W. L. Nighan, "Electron Energy Distributions and Collision Rates in Electronically Excited N_2, CO, and CO_2," *Physical Review A*, Vol. **2**, No. 5 (1970), pp. 1989–2000.
[8] B. E. Cherrington, "Gaseous Electronics and Gas Lasers," Pergamon Press, NY (1979).
[9] G. J. Schultz, "Resonances in Electron Impact on Diatomic Molecules," *Reviews of Modern Physcis*, Vol. **45**, No. 3 (1973), pp. 423–486.
[10] V. L. Ginzburg and A. V. Gurevich, "Nonlinear Phenomena in a Plasma Located in an Aiternating Electromagnetic Field," *Soviet Physics*, Uspekhi **3**, Nauk 70 (1960), pp. 115–146.
[11] K. Kuriki, I. Kimura, and Y. Arakawa, "Laser Propulsion (LAP)," *Proceedings of Space Station Symposium, Japan*, B-19 (1982).
[12] K. Maeno, "Advanced Scheme of CO_2 Laser for Space Propulsion," *Space Solar Power Review*, Vol. **5** (1985), pp. 207-211.